SSPS TECHNICAL REPORT No. 6/81

Determination of the Spectral Reflectivity and the Bidirectional Reflectance Characteristics of Some White Surfaces

by

G.P. Görler
D F V L R
Federal Republic of Germany

Prepared for

IEA - OPERATING AGENT DFVLR, Köln
O.A. Supervision: Dr. M. Becker

Foreword

All activities concerning optical flux measurements near the aperture plane of the CRS receiver depend on certain assumptions. A very essential one is that of a completely diffuse light reflection on the prepared outside of a moving target.

The DFVLR Institute for Space Simulation has made available its test capacities for the investigation of influence parameters. The efforts were directed towards spectral, angular, and temperature effects. Some different target materials were used. The main part of the treatise, however, concentrated on the plasma-sprayed ceramic from EIR, Switzerland, applied both at the FAS-EIR and at the HFD-DFVLR targets.

All results including the expectable degradation indicate that immediate calibration measurements of the actual target and its circumstances are very important.

Determination of the Spectral Reflectivity and the Bidirectional Reflectance Characteristics of Some White Surfaces

Abstract

Each of the heliostats forming the mirror field of a solar thermal power plant with central tower will generate an image of the sun on the entrance of the central radiation receiver. The quantitative determination of the integral power within this image and its distribution is necessary to check the performance of the mirror array as well as the efficiency of the receiver and the subsequent thermodynamic process. At the solar power plant built by the IEA near Almeria (Spain), a part of this problem is to be solved by viewing the brightness of white surface elements on a movable traverse scanning the image in the entrance area of the receiver cavity.

Measurements of the spectral reflectivity and of the spatial distribution of reflected intensity at various angles of incidence were carried out on a sample of this coating. The results are compared with the properties of some other white surfaces. Additionally, the effect of varying temperature of the sample on the spectral reflectivity and its angular distribution was studied as well as the dependence of angular distribution on the wavelength.

Contents

1. Introduction

A solar thermal power plant designed as solar tower - central receiver system - is made up of two essential components: One component is the heliostat field with its problems concerning focussing, heliostat tracking, reflection characteristics of the individual heliostats as well as their long-term stability, etc.; the other component is the receiver with the subsequent heat engine for which the receiver is the high temperature level heat source. The interface between the two components is the entrance aperture of the receiver. The radiation coming from the heliostat field and passing through this area is the primary thermal power which, beyond the interface, appears again in the form of power losses of the receiver, other losses, waste heat, and finally useful power.

Assessment of the capability of the heliostat field as well as determination of the efficiency of the receiver including thermodynamic process calls for a quantitative measurement of the integral radiation flux through the interface. At the IEA solar thermal power station of the solar tower type built near Almeria/Spain under DFVLR project management, a movable traverse with a row of radiometers will to this purpose scan the radiant flux in the entrance aperture of the receiver and its distribution. The surface of the traverse between the sensors is to be coated with white, diffusively reflecting elements. In this way, it is in addition possible to get an independent measure of the radiation distribution by viewing - during scanning of the cavity - the local brightness from an adequate direction with an electronic camera and by subsequent image processing. Fig. 1a shows the plane scanned by the traverse. The sun's image generated by the heliostats appears in the figure on the closed door of the receiver which is placed in front of the entrance aperture to protect the receiver during non-operation periods and to reduce the thermal losses of the coolant. For the same purpose of heliostat alignment, a more indirect approach was chosen in the solar power station EURELIOS of the E.C. near Adrano/Sicily: For

measurements, each individual heliostat unit is tilted by a certain angle and oriented to a fixed square target screen below the receiver entrance aperture (see Fig. 1b), where the radiation distribution and its integral can be determined.

The objective of the present investigation was to gather quantitative data for the optical properties of the white surface elements of the traverse. Ideally, the following requirements are imposed on such a coating:

1. High reflectivity for solar radiation.

2. Within the spectral subinterval cut out of the complete terrestrial solar spectrum by the characteristic of the wavelength-dependent sensivity of the camera, the reflectivity must be wavelength independent, i.e. the surface must not exhibit any spectral selectivity within this interval.

3. The reflectivity must be independent of the angle of incidence of the radiation; this requirement is important since, due to the dimensions of the heliostat field, the sources of the incident radiation are distributed onto a large solid angle range.

4. The spatial distribution of the reflected radiation must be a cos-distribution; in this ideal case (ideally diffuse reflection; perfectly diffuse radiator), the surface brightness on the traverse observed by the camera is independent of the angle of observation.

5. The spatial distribution of the reflection must be independent of the angle of incidence (this property exists if the conditions 3 and 4 are both fulfilled) and it must be independent of the wavelength.

6. In addition, the reflectivity as well as the spatial distribution must be independent of the surface temperature; this condition is necessary as the traverse must be anticipated to experience a marked increase in temperature - even if the reflectivity is near 1 and scanning of the receiver aperture is performed fast.

Of course, a real surface cannot be hoped to fulfill all of these idealizing conditions. But the various desired characteristics may in practice be approximated, though not all to the same degree. An almost wavelength-independent high reflectivity over an interval, which e.g. with a silicon target camera is limited to the 0.4 - 1.1 μm range, is exhibited by numerous surfaces; one example is the well-known MgO coating (Fig. 2). The condition calling for a simultaneous temperature independence of the coating confines the number of candidate materials. As seen from this point of view, particularly ceramic surfaces seem to be suited for use. The three samples employed for the present investigation were made of this material. That sample, which was considered as the actual test object from the beginning and on which most of the measurements were conducted, was a plasma-sprayed Al_2O_3 coating on an aluminium base.

A characteristic which is more critical than the uniformity of the reflection over a wavelength range is the spatial distribution of the reflected intensity, i.e. the approximation of the ideal diffuse surface. What may be expected is shown by Figs. 3a and 3b, taken from the literature /Ref. 1/ using as an example the MgO layer which in general is regarded as a good approximation of a diffuse reflector.

Already at a vertical incidence of light ($\vartheta_e = 0^o$), we observe deviations from the cos-law which at increasing angle of observation become quite distinct. If the angle of incidence ϑ_e gets large, these deviations turn out to be very marked.

Before we set out to compare these published values with the results of the measurements carried out on our samples, some remarks need to be made yet on the definition of reflectivity, on the reduction of the test parameters, and on the measuring equipment.

2. Definition of the reflectivity; reduction of the measurement parameters

The four basic approaches to be used for determining the reflectivity of a surface are presented in Fig. 4a-d. Complete information on the reflection behavior is obtained by measurement according to the procedure 4a; this approach, however, calls for variation of the 4 variables $\vartheta_e, \varphi_e, \vartheta$ and φ - even at constant temperature and fixed wavelength. The other three procedures each represent subintegrals and/or complete integration over the reflectance curves. The cases 4c and 4d are based on the assumption of an uniform distribution of the radiation incident from the hemisphere.

The variety of the characteristics to be measured is, however, reduced by symmetry relations: the arrangement 4a is symmetrical in the variables (ϑ_e, φ_e) and (ϑ, φ); furthermore, reciprocity exists between the arrangements 4b and 4c. More detailed information is found in /Ref. 2/. A reflectivity, which can be expressed by a dimensionless number $0 < \varrho < 1$, is (for a defined wavelength and sample temperature) only obtained by measurement according to Fig. 4d. Such an arrangement is, however, hardly suited for experimentation; in addition, it does in most cases not correspond to the real problem. For a surface, whose reflectivity is independent of the direction of the incident radiation, the arrangement 4b (and because of the reciprocity relation also arrangement 4c) supplies the desired value. The spectral photometer used in the present investigation incorporates the arrangement 4 c - with the additional condition $\vartheta = 0^o$.

In general, however, neither the amount of the reflectivity nor the distribution of the reflected light are independent of (ϑ_e, φ_e). Under such circumstances, the complete function $\varrho'' = \varrho''(\vartheta_e, \varphi_e; \vartheta, \varphi)$ $\quad - \lambda$ and T being fixed - must be determined. A reflectivity $\varrho'(\vartheta_e, \varphi_e)$ just dependent on the angle of incidence is achieved from the function by integrating over ϑ and φ; integration may also be performed in the device itself by means of an Ulbricht sphere ("integrating sphere").

For samples, which neither exhibit a macrostructure of their surface (e.g. profile) nor a preferential orientation in microscopical scale (texture of the surface; orientation of the crystallites of a pigment), the dependence of the reflection on the angle of incidence (ϑ_e, φ_e) is reduced to a dependence on the angle ϑ_e against the surface normal. For the reflected radiation, an azimuthal dependence must not be neglected, as - except for vertical incidence - a plane is determined by the direction of the incident radiation and the surface normal, which by itself already defines a preferential direction for the azimuth angle.

In our investigation, we assume that the camera observes the traverse under a fixed angle ϑ against the surface normal of the receiver aperture. If we take the thus defined section to the origin of the angle scale φ_e, the sources of the incident radiation are distributed to a large range (ϑ_e, φ_e). As furthermore the temperature T of the surface and the wavelength may be included as parameters in the measurement, it is quite evident that a quantitative determination of all characteristics of the reflection behavior would already for a single sample involve a very extensive measuring program. In practice, measurement must be confined to a few key points. The present investigation covered the following measurements:

1. The wavelength-dependence of the reflectivity was measured in a geometrical standard arrangement defined by the spectral photometer. By the use of an Ulbricht sphere, the sample is exposed to a diffuse hemispherical illumination; reflection is observed in normal direction. The resulting curve $\varrho(\lambda)$ was checked for a possible temperature-dependence by investigating the sample once at T_r, then at two increased temperatures (100° and 130° C).

2. To investigate the angular dependence, the reflection distribution was first measured at normal illumination. Then, corresponding curves were plotted for various angles of incidence. The upper limit is given by the geometry of the solar thermal power station, where the maximum angle between the normal of the receiver aperture and the heliostats at the edge of the mirror field is approx. 40°. The angle of observation, ϑ, of the measurement is inside the plane put up by the cavity normal and the angle of incidence; in practice, it will be outside this plane. Taking also into consideration the azimuthal dependence of the reflection, however, would at once multiply the number of necessary measuring curves. But this neglect does not entail a significant disadvantage, since the additional dependence is not very marked, as is demonstrated by the good approximation to a diffuse reflection behavior following from the measurements.

The spectral region used to investigate this spatial distribution of the reflection is defined by the light source spectrum and the spectral response of the detector. Therefore, measurement covers mainly the region of the red light and of the adjacent near infrared. To examine whether the distribution is wavelength-dependent, a short-wave part was cut out of this spectrum by means of a blue-green filter. This part was again used to plot a curve $\mathcal{F}(\vartheta)$.

For determining the temperature dependence, the reflection distribution of the surface was investigated both at room temperature and for increased sample temperatures (T= 100° C; T = 150° C).

3. Measuring equipment

The spectral reflectance was measured by the use of a commercial spectral photometer (Zeiss company; model PM Q II). It is composed of a monochromator M 4 Q III, whose wavelength ranges from less than 300nm to 2.5 μm, and of the reflectance attachment RA 3, comprising an integrating sphere 10 cm in diameter. The sample rests on a section of the sphere whose internal wall is illuminated evenly by an incandescent lamp. The intensity reflected by the sample in the direction of the

surface normal is observed. It is compared with the brightness of the sphere's wall, which is used as internal standard. Hence measurement yields a relative reflectivity.

By determining the reflectivity of a fresh MgO coating, the curves $\varrho(\lambda)$ obtained for the investigated samples can be converted into absolute values.

For determination of the angular distribution of the reflection, the sample is first mounted vertically on a blackened support. On the sample, a spherical field about 6 cm in diameter is illuminated. To this purpose, a diaphragm opening covered by a diffuse foil and illuminated by an incandescent lamp is imaged on the sample. At a light source distance of about 90 cm from the sample, the divergence of the incident beam is small. The incandescent lamp is operated with reduced power (0.6 A constant current at about 5 V voltage drop, i.e. with 3.0 W), as at rated power (6 V/5 W) the decrease in brigthness led to a drift of the measurement values already in the course of the measurement.

The detector is placed level with the sample on an arm rotatable about an axis whose extension goes through the center of the observed measuring field. Angular setting is made by means of a circular arc bar with graduation whose distance from the axis is at the same time its radius of curvature (R=114.6 cm). This geometrical arrangement, while requiring little effort, allows a very accurate angle setting; its major advantage is that the observation angle ϑ of the detector can be approximated very closely to the angle of incidence ϑ_e. (An available commercial goniophotometer has - besides some others - the essential disadvantage that a gap of at least 27° must remain between ϑ_e and ϑ, an interval which hence is not accessible to measurement. With the arrangement as used, this difference can be reduced to about 3°).

The detector's field of view is in each angular position larger than the illuminated field, so that for an ideally diffuse surface the signal would be $S \sim \cos \vartheta$ with increasing angle of observation ϑ. (The opposite arrangement, as realized in a previous investigation (cf. /Ref. 3/), where the solid angle covered by the detector defines the measuring field on the evenly illuminated sample, leads for the same ideal surface to a signal which is independent of ϑ. But this second arrangement has certain disadvantages; it namely requires a markedly greater sample surface). As the primary light beam was not chopped and as no lock-in amplifier was used on the detector side, measurement must be performed in a dark room.

As detector, use is made of a silicon photodiode (BPW 20) with a photosensitive area of 7.5 mm^2. Measurement uses the short-circuit current which is generated by the incident radiation. This yields an output signal which is strictly proportional to the brightness over a minimum of 7 decades (exceptionally, similar diodes achieve about 11 decades) (cf. Fig. 5). The circuit which supplies the output signal proportional to the short-cicuit current recorded on a plotter is represented in Fig. 6.

Apart from geometrical factors and a possible modification by the reflecting surface, the signal is proportional to the convolution integral of the curves for the spectral response of the photocell (see Fig. 7a) and the spectral intensity distribution of the incandescent lamp, which will be similar to the standard light spectrum of a tungsten lamp of T = 2850 K (cf. Fig. 7b). The product of both distributions is a curve with a marked maximum approximately at the red limit of the visible spectrum. By increasing the heating power of the incandescent lamp, it may to a certain degree be shifted towards shorter wavelengths. A considerably greater shift of the spectrum - at the expense of a substantial intensity drop, however, - is brougth about by an optical filter which blocks the red and the adjacent infrared component. The transmission characteristic of the filter BG 23 (Schott; Spindler & Hoyer) used in the present investigation, which entailed a signal attenuation down to 4.20%, is illustrated in Fig. 8.

In order to determine the temperature dependence of the optical properties, a Pt-100 foil resistance thermometer, which was some tenths of a millimeter thick, was attached to the back of the sample. During the measurements, it was connected in 4-wire technique to a digital temperature indicator. Stuck onto this was a Kapton foil heater whose size corresponded almost exactly to the sample surface so that the heating power per unit of surface area could be kept at a low level and temperature gradients in the plane of the sample could be prevented. As the sample itself consisted of coated aluminium, the temperature drop from the back to the front is negligible under the accuracy requirements applicable in our case. Backside heat losses were reduced by means of several layers of ceramic paper.

4. Measurements on the spectral reflectivity

Investigation of the spectral reflectivity included the following surfaces:

a) Sample I (Real/EIR-Würenlingen).

This sample, which is the actual object of the present investigation, is an aluminium substrate 10.0 x 12.3 cm^2 in size, whose front is coated with plasma-sprayed Al_2O_3. The back is uncoated and shows an uniformly mat, relatively rough structure obviously resulting from sand blast treatment;

b) Sample II (Remus/DFVLR-NE/OE).

The sample is a white ceramic tile 10 x 10 cm^2 in size with glazed, uneven surface;

c) Sample III (Dr. Köhne/DFVLR-EN-TP).

This smaller (approx. 7 x 7 cm^2 great) almost white ceramic tile has a mat, even surface.

The investigated spectral region ranges from 360 nm to 2.5 μm and thus covers the whole terrestrial solar spectrum.

The relative reflectance of these 3 samples, related to the internal standard of the spectral photometer used for measurement, is listed in each case for two measurements apart in time in Table 1. The two curves obtained for sample II agree exactly within the reproducibility limits of the device, i.e. $\pm$ 0.25%. For sample III, a slight degradation is observed which is confined to the short-wave range up to 500 nm. A more marked decrease of the reflectivity, at considerably higher initial values, is exhibited by sample I in the short-wave subinterval up to about 600 nm. In the course of the subsequent investigations on the angular dependence of the reflection on this sample, the reflectivity decreases further due to degradation, as is shown in Table 5 at the bottom.

The characteristic, obtained in the same way, of the relative spectral reflectivity of a fresh, thick magnesium oxide coating is depicted in Table 2. Also presented is the characteristic of the absolute spectral reflectivity of such a surface taken from the literature, whose residual incertainty is about $\pm$ 0.01; a subinterval of this curve has already been given in Fig. 2. Comparison of the measured relative values with the absolute characteristic yields a calibration function by means of which the values obtained for the unknown surfaces can be converted into absolute values. The resulting curves of the absolute spectral reflectance of the samples I, II, and III are also listed in Table 2. For the sample I, this curve is represented in Fig. 9.

The uncertainty of the measurement results is just given by the residual error of the standard used for calibration as well as by the additional minor error due to equipment. This is, however, based on the assumption that the unknown surface as well as the standard represent a good approximation to a diffuse reflector. This condition is fulfilled by the samples I and III, but not by sample II which, as is seen in the Fig. 15 below, shows an approximated specular reflex. For such surfaces, the spectral photometer, due to the construction of the reflectance attachment yields too small a reflectivity. Although it is possible to increase the reliability of the absolute conversion also for these types

of surfaces, any efforts to this purpose were not undertaken in the present investigation, as the sample II is not suited for the intended use by virtue of its reflection distribution.

5. Measurements on the angular dependance of the reflection

For the spectral reflectance curves of diffuse surfaces, comparison with a MgO standard provides conversion into absolute values. Such a comparative standard is not available for measurement of the angular dependance of the reflected radiation; therefore, the reliability of the distribution curve is bound to the reliability of the used measuring set-up. To exclude the possibility of a systematic error distorting the measurement curves, some preliminary investigations were carried out.

Fig. 10 shows the measured relative intensity distribution as a function of the angle of observation ϑ for two surfaces, one of which was coated with "Nextel Velvet Coating" 2010 (white), while the other one consisted of a thin MgO layer on a copper plate; the angle of incidence was $\vartheta_e = 0^o$ in each case. Also plotted is the characteristic of an ideal cos-distribution. Both coatings reveal a preferential reflection in the range $\vartheta \simeq 0^o$ as well as in the range of larger angles in increasing deviation from the ideally diffuse reflection behavior. This deviation shows more clearly if the quantity $S(\vartheta)/\cos\vartheta$ is plotted as ordinate, which in our measuring set-up would be constant for the ideally diffuse reflector. Fig. 11a gives the reflection distribution of the MgO coating in this type of plotting. Except for the reflection maximum within an angular range of about 10^o around the angle of incidence $\vartheta_e = 0^o$, attributed to a residual component of nearly specular reflection on the baseplate (due to insufficient thickness of the MgO coating), the decrease of the reflection towards greater angles corresponds approximately to the characteristic as obtained from the values given in the literature (cf. Fig. 3a/b). The reflection distribution of the Nextel coating in the same way of representation is plotted in Fig. 11b (curve 2). This figure includes in addition the direct measuring signal of a previous measurement on the same surface (cf. /Ref. 3/), (curve 1), where the geometrical arrangement, as mentioned above, was chosen such

that an ideally diffuse surface would have given an angle-independent signal. The curve obtained with the present set-up is largely identical with the previous measurement; the variations in the range of large angles and in the vicinity of the angle of incidence are resulting from the fact that, first, the angle of incidence in the previous measurement was $\vartheta_e = -2^o$ and, second, with the new arrangement the angular uncertainty ($\Delta\vartheta_e, \Delta\vartheta$) is considerably smaller.

The reflection maxima in the vicinity of $\vartheta = 0^o$ occurring both with the magnesium oxide coating and with the Nextel sample are of different character: While for the MgO coating the maximum moves towards $-\vartheta_e$ with increasing angle of incidence ϑ_e, for the Nextel coating the maximum is shifted towards $+\vartheta_e$, i.e. it always appears in the direction of the angle of incidence. This phenomenon of retroreflection (cat's eye effect, Scotchlite effect) is a property of the pigment containing a certain amount of very fine glass or quartz spheres.

Fig.12 shows a reflectance measurement on sample I for $\vartheta_e = 0^o$. It is obvious that it is largely in agreement with the characteristic plotted in Fig. 10 for the MgO and the Nextel surfaces.

How small the practical effects of the deviation from the ideally diffuse reflection are, is shown more clearly by representing the reflectance in a polar coordinate diagram ("indicatrix"). The distribution for $\vartheta_e = 0^o$ and $\vartheta_e = -10^o$ measured on sample I is given in this form in Fig. 13. As is known, the reflection distribution of the ideally diffuse surface corresponds in this diagram to a circle.

Fig. 14 shows the distribution of the reflection on sample I, when the angle of incidence is changed from $\vartheta_e = -10^o$ via -20^o and -30^o to -40^o. In the direction of the normal of the sample surface we observe a decrease of the reflected intensity, while in the vicinity of $\vartheta = -\vartheta_e$ there is a slight increase. The associated measured values are listed in Table 3 in direct units of the signal quantity. Since the integral intensity of the illuminated measuring field was kept constant in this case, the 4 curves also give a correct indication of the quantitative

ratio of the reflection distributions. In general, the ordinates of the figures present the distribution only in arbitrary units. In those cases where a normalized representation was selected, the signal observed at a distance of 10° from the angle of incidence was taken for normalization ($S(\vartheta)/S(10^o)$ for $\vartheta_e = 0^o$ or $S(\vartheta)/S(0^o)$ for $\vartheta_e = -10^o$), as e.g. with vertical incidence, because of the above-mentioned necessary minimum angle between light source and detector, observation can only start beyond 3°.

Remains to be clarified to what extent the reflectance observed on the sample I varies with the wavelength of the radiation used for the investigation. It cannot be expected that there is a complete independance within the whole spectral region from 0.36 to 2.5 μm, as is already gathered from the literature data for the MgO coating (Fig. 3a/b). The result obtained on our sample is listed in Table 4. Initially, the incandescent lamp first operated with undervoltage was turned up to about rated power. This gives rise to a shift towards blue of the source spectrum, accompanied by a signal rise to 218 %. Then, the component of the red light and of the NIR was suppressed by the filter BG 23, with the signal decreasing to 4.20 %. The angular distribution of the reflected radiation for all three spectra, at an angle of incidence of $\vartheta_e = -10^o$, is listed in the first 3 columns of the table. The next 3 columns give the distributions normalized to $S(0^o)$, which allow a direct comparison of the relative reflectance. A weak tendency of a wavelength-dependence is observed, but the differences, which do not exceed the order of magnitude of 0.5 %, are within the limits of the measuring inaccuracy and without any significance for practical applications.

A completely different reflection distribution is exhibited by sample II - in spite of its uneven surface. Measurement, represented in Fig.15, indicates already for $\vartheta_e = 0^o$ the descent of an approximate specular reflection maximum. At an angle of incidence $\vartheta_e = -10^o$ we have a complete picture of the reflection maximum whose peak value is a factor of 10 higher than the intensity of the approximate diffuse component. The

half-width of the reflection maximum is 8°; hence, it is considerably greater than that of the incident light beam, whose angular divergence is below 2°. This spread of the specular reflected beam is a consequence of the sample's surface structure. When integrating over the hemisphere, the quantitative component of the approximate specular reflected light in the total reflected radiation decreases very much compared to the diffuse component, as the reflection maximum takes only a small part of the solid angle, in spite of its broadening. Nevertheless, the specular reflection component is still disturbingly great. The application of a surface with such a reflection characteristic for the desired use is ruled out right from the beginning.

6. Reflection measurements at increased sample temperature

Just as on the wavelength of the radiation, the reflectance of a sample can also be dependent on the surface temperature which, in addition, may affect the characteristic of the spectral reflectance. For sample I, whose surface coating consists of the high-temperature material aluminium oxide, any noticeable effects of a temperature change over a limited interval are not anticipated. Nevertheless, this question should be handled further, as the surface will experience a marked temperature increase during practical operation.

Table 5 presents a juxtaposition of a group of 4 measuring series 3 a-d on the spectral reflectance and the two preceding measurements. First, the sample was measured again without additional heating; then, two measuring series were carried out at temperatures of 100° C and 130° C; finally, following cooling down of the sample, the spectral reflectance was measured once more. Compared with the previous measurement 2, the curve 3a shows a further decrease of the reflectance by about 0.5 % which covers the whole spectrum - except for the short-wave range, where a slight increase is observed this time. The influence of sample heating (curves 3b and 3c) is restricted almost exclusively to the short-wave region; the minor change observed does not seem to be completely reversible, as is indicated by the following curve 3d.

Generally, the effect of temperature is just a little beyond the measuring uncertainty which increases towards the measuring range limits of the spectral photometer. The slight influence on the measurement may be attributed to an absorbed H_2O component in the coating.

After completion of all measurements, the coating of sample I was cleaned, dried and measured again. The measuring series 4 indicates to what extent a slow degradation of the surface can be eliminated by this treatment.

Besides the effect of temperature on the spectral reflectance, a possible effect on the distribution of the reflected intensity was investigated. The result is shown in Table 6. In addition to two previous measurements at room temperature (measuring series 1 and 2), the table first lists a renewed measurement at T_Z (measuring series 3a); the two following measurements (measuring series 3b and 3c) present the characteristic at a sample temperature of 100° and 150°C, respectively. The angle of incidence was $\vartheta_e = -10°$ in each case. The lower part of the table gives the measurements in normalized form, related to $\mathcal{F}(\vartheta = 0°)$; juxtaposed are the values found for a perfect cos-distribution. The variation, exhibited by the individual measuring series at different sample temperatures, exceeds nowhere the order of magnitude of some 10^{-3}, i.e. it is completely within the limits of the measuring uncertainty. Hence, any possible effect of the temperature on the distribution of the reflected radiation is beyond measurement in the approach used in this investigation; its consequence with respect to the practical utilization of the sample must remain infinitesimal.

7. Conclusion

The results obtained for sample I, the primary object of the present investigations, indicate a reflection behavior corresponding to the requirements imposed on an approximate diffusely reflecting white surface. For sample II, however, measurement finds out a considerable specular reflection component, so that this surface is not qualified for the envisaged use. On sample III, which is intended for a similar

application and whose surface is diffusely mat, such a detailed measurement of the angular distribution of the reflected radiation was not performed, as a definition of the measuring parameters is not available as yet.

The absolute spectral reflectivity meaasured for sample I is listed in Table 2 and in Fig. 9. The effective reflectivity

$$\varrho_{eff} = \frac{1}{S_0} \cdot \int_{\lambda_1}^{\lambda_2} \varrho(\lambda) \cdot S(\lambda) \cdot d\lambda$$

is only obtained from this curve when the spectral density $S(\lambda)$ of the incident solar radiation is known. A measure of this quantity, from which follows, among others, the integral power absorbed in the coating, is derived according to Fig. 16 from a weighted representation based on the frequently applied AM2 spectrum according to P. MOON. As is shown in this type of plot, the reflectance of the sample I over the wavelength interval important in terms of energy is sufficiently high and uniform.

Investigation of the temperature-dependence of the spectral reflectivity yields a weak effect which is confined to the short-wave part of the spectrum and which can be explained e.g. by a little amount of water absorbed in the coating.

More critical is the angular dependence of the radiation reflected on sample I, for which deviations from the cos-law are already observed for vertical incidence of radiation. In addition, a - though weak - dependence of the distribution from the angle of incidence is found which was varied up to 40^{o}. But the deviation of the reflection distribution from that of an ideally diffuse surface is within the limits of deviation also identified for other surfaces considered to be good approximations to a diffuse reflector.

There is only a very small dependence of the distribution on the spectral composition of the radiation used for measurement over the limited wavelength region of interest in this case. Any dependence on the surface temperature of the sample is not observed within the measuring accuracy limits.

To determine the relative power distribution in the sun's image generated by the individual heliostats in the entrance aperture of the receiver, the reflection distribution of the sample as measured in the present investigation is sufficient, which approximates the angular distribution of a diffuse reflector. For a quantitative determination of the integral power through an evaluation of the absolute area brightness and its variation over the receiver aperture as observed by the camera, the measuring parameters investigated here are not sufficient. Such a quantitative application requires knowledge of the complete function $\varrho'' = \varrho''(\vartheta_e, \varphi_e, \vartheta, \varphi)$ with a certain minimum accuracy. Then, the extension of the heliostat field in the direction ϑ_e and φ_e relative to the surface normal of the receiver entrance aperture necessitates - even at a given position of the viewing camera - basically a double infinite manifold of measuring values. Although the fixed arrangement of the 100 heliostats relative to the radiation receiver reduces this multiplicity, the measuring problem still is so extensive that preference is given to in-situ calibration by means of a light beam of defined power, which is directed from each location of the individual heliostats to the traverse.

One problem in applying surface elements like sample I will be the degradation with time of the surface properties. It will hardly affect the reflectance distribution, but will cause a marked decrease of the spectral reflectivity. This problem, however, concerns all coatings which are required to show diffuse reflection and which therefore must not have a microscopically smooth (e.g. glazed) surface.

8. Literature

/1/ R.C. ZENTNER, R.K. MacGREGOR, J.T. POGSON — Bidirectional reflectance characteristics of integrating sphere coatings

/2/ R. SIEGEL, J.R. HOWELL — "Thermal Radiation - Heat Transfer"
McGraw-Hill Book Co., New York 1972
and: NASA SP-164, Vol. I - III, Washington, D.C. 1968

/3/ G.P. GÖRLER — Reflexion an Kaltwandoberflächen für Strahlung im sichtbaren Bereich
Internal Report (DFVLR) IB-353-74/48 (1974)

Fig. 1a Central receiver with closed shutters at the Almeria CRS solar power station

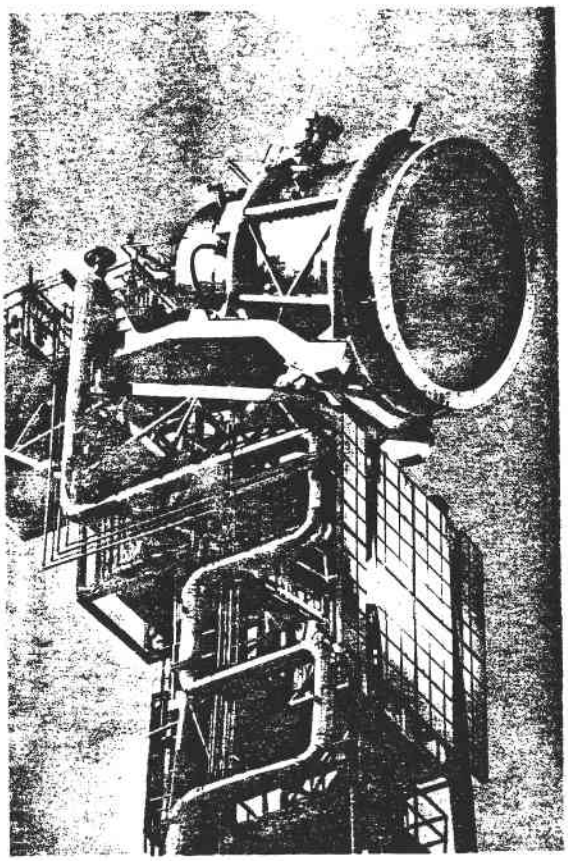

Fig. 1b
Receiver and projection screen at the EURELIOS solar power station

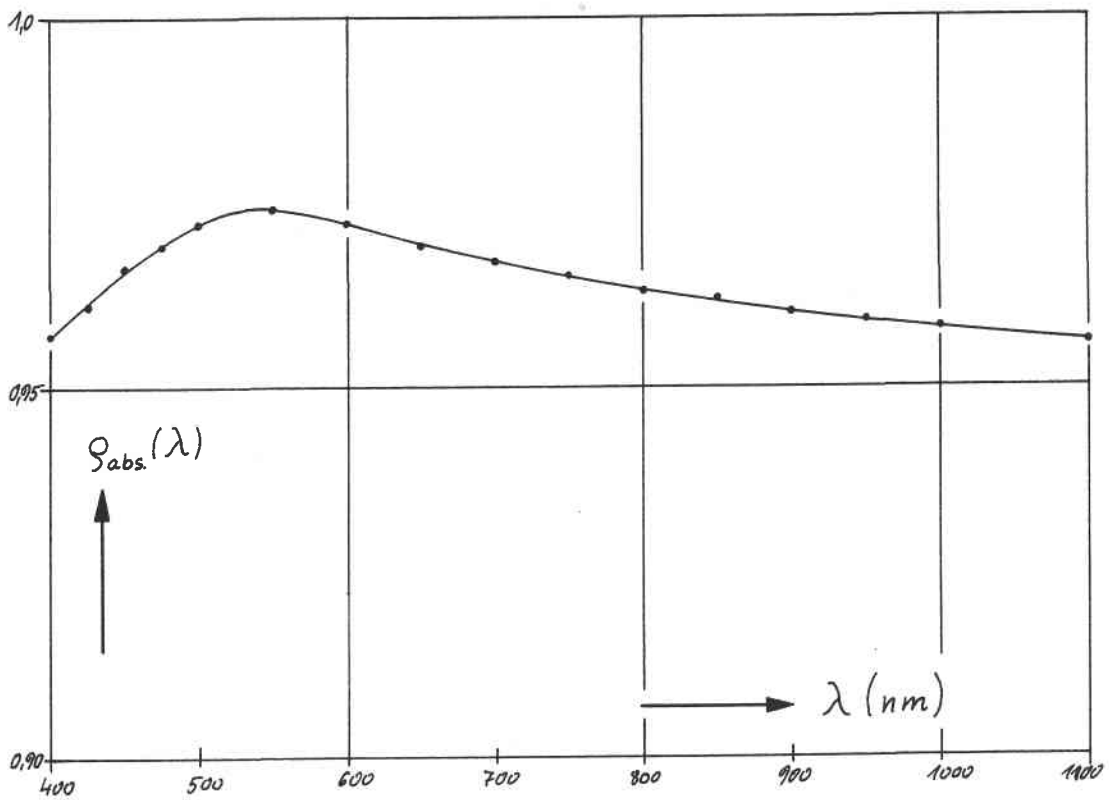

Fig. 2 Absolute spectral reflectivity of magnesium oxide in the wavelength range from 0.4 to 1.1 µm

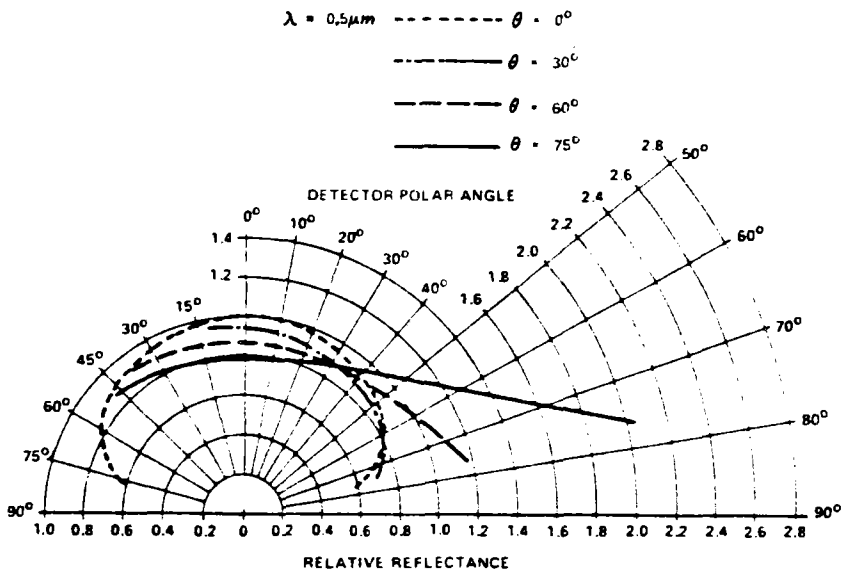

Fig. 3a Directional reflectance characteristics of magnesium oxide for a wavelength of 0.5 μm (referred to $\mathcal{F}(\theta_e = 0, \theta = 0)$)

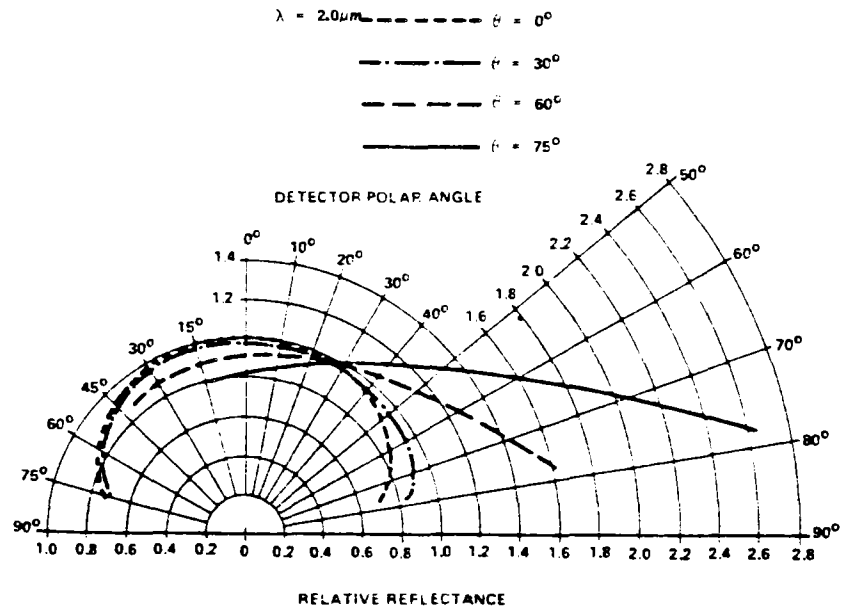

Fig. 3b Directional reflectance characteristics of magnesium oxide for a wavelength of 2.0 μm (referred to $\mathcal{F}(\theta_e = 0, \theta = 0)$)

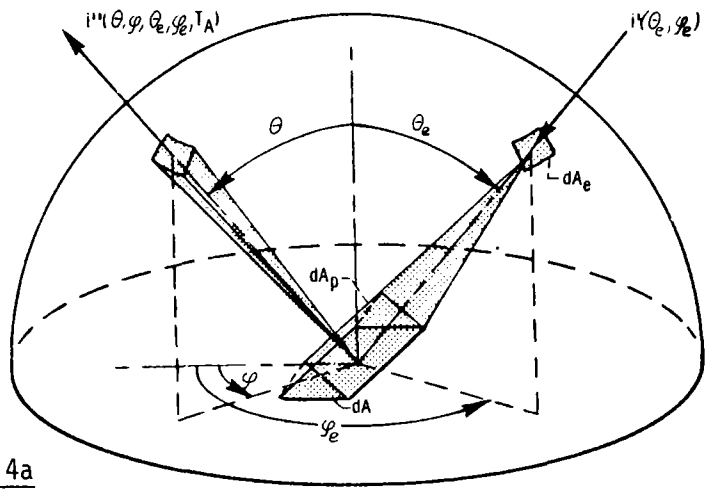

Fig. 4a

Bidirectional reflectivity ρ'' (θ, ϕ; θ_e, ϕ_e; T_A)

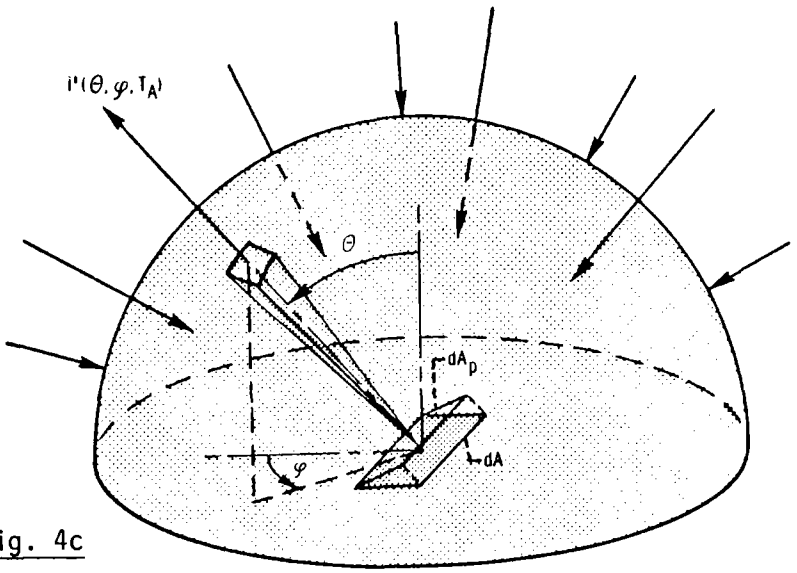

Fig. 4c

Hemispherical-directional reflectivity ρ' (θ, ϕ; T_A)

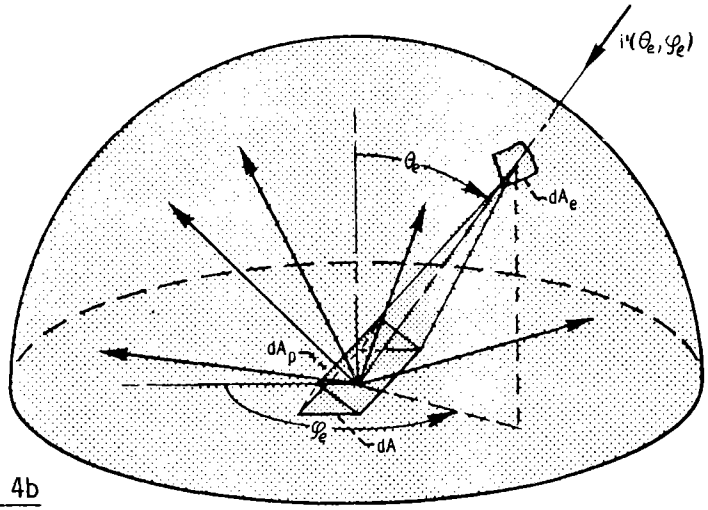

Fig. 4b

Directional-hemisperical reflectivity ρ' (θ_e, ϕ_e; T_A)

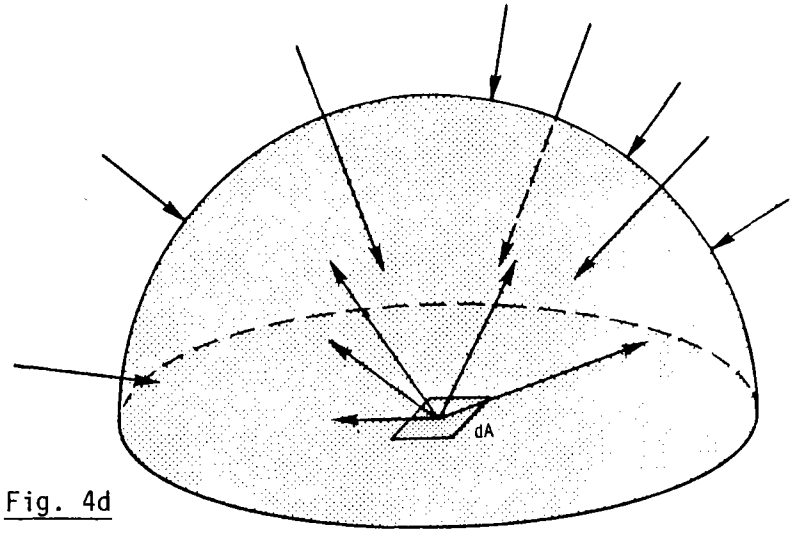

Fig. 4d

Hemispherical reflectivity ρ (T_A)

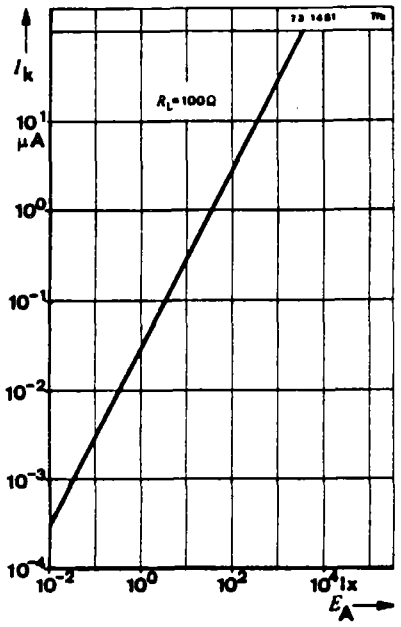

Fig. 5
Short circuit photocurrent vs. illuminance for the silicium photodiode in photovoltaic mode

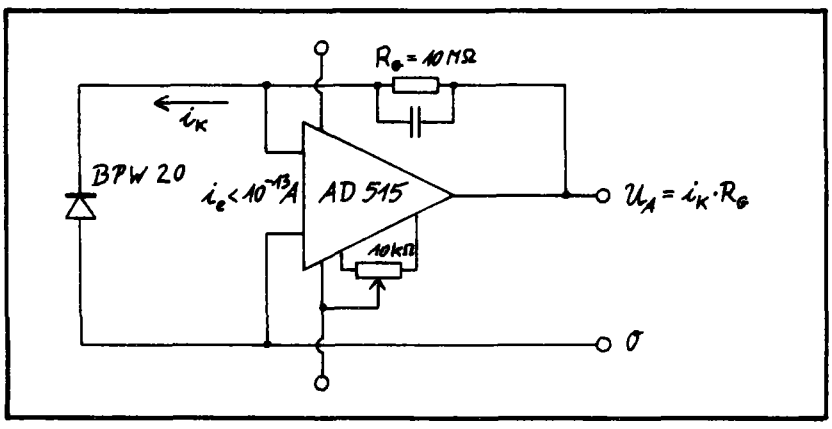

Fig. 6 Op-Amp connection for conversion of short circuit photocurrent to a proportional output voltage

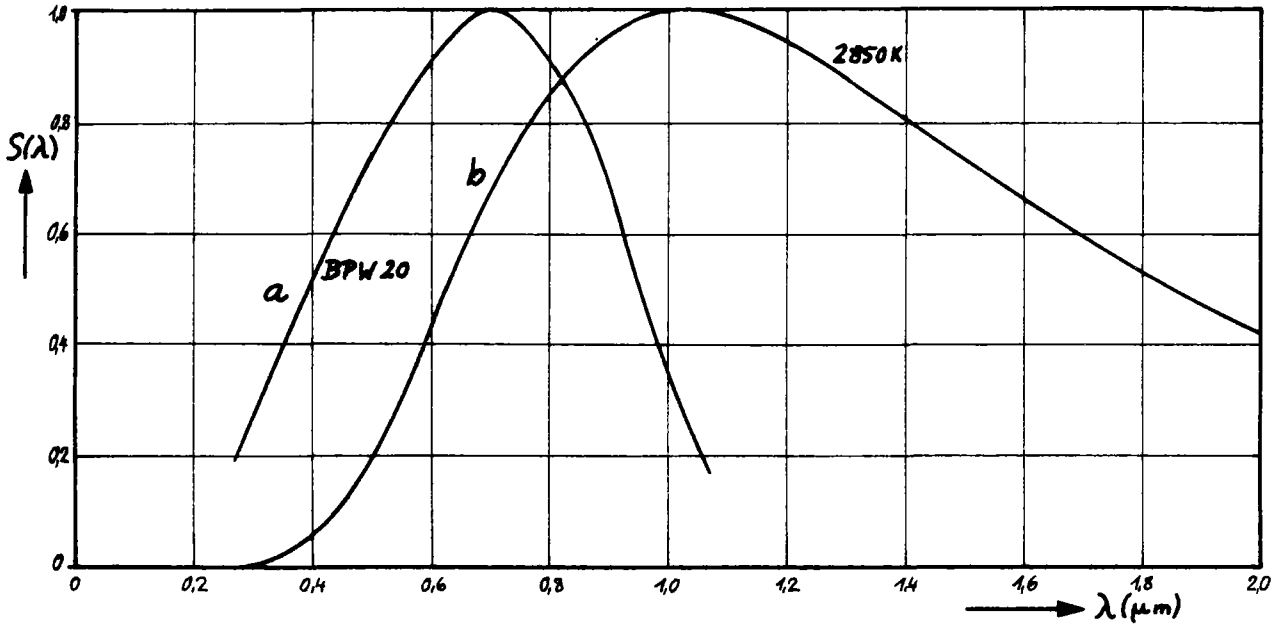

Fig. 7 Spectral response characteristics of the photodiode BPW 2o (curve a) and relative spectral intensity distribution of a filament lamp of 285o K (curve b)

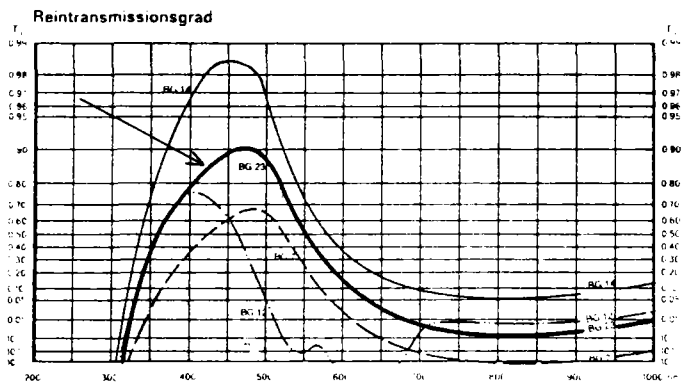

Fig. 8 Spectral transmittance of the filter BG 23

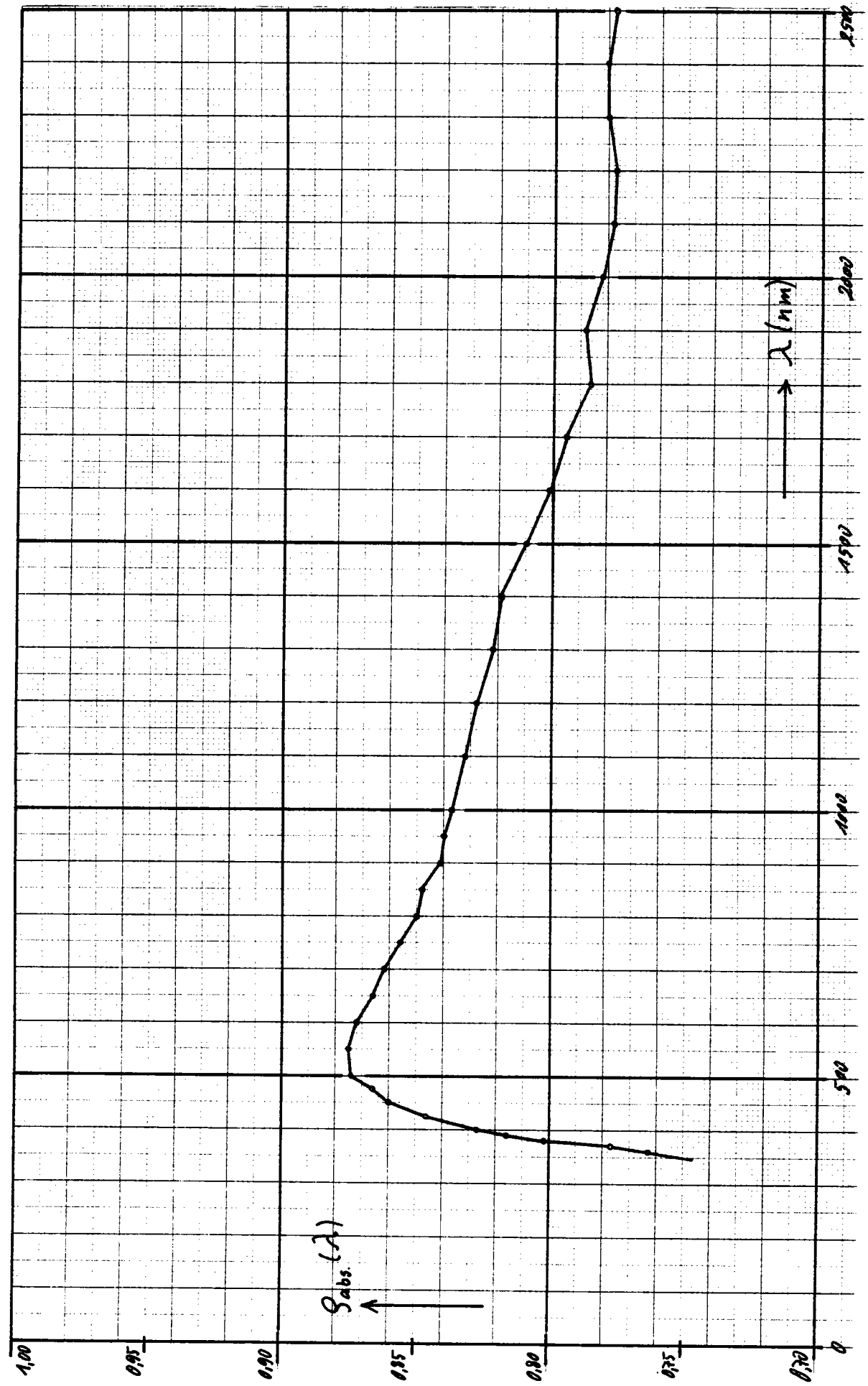

Fig. 9 Absolute spectral reflectivity of sample I

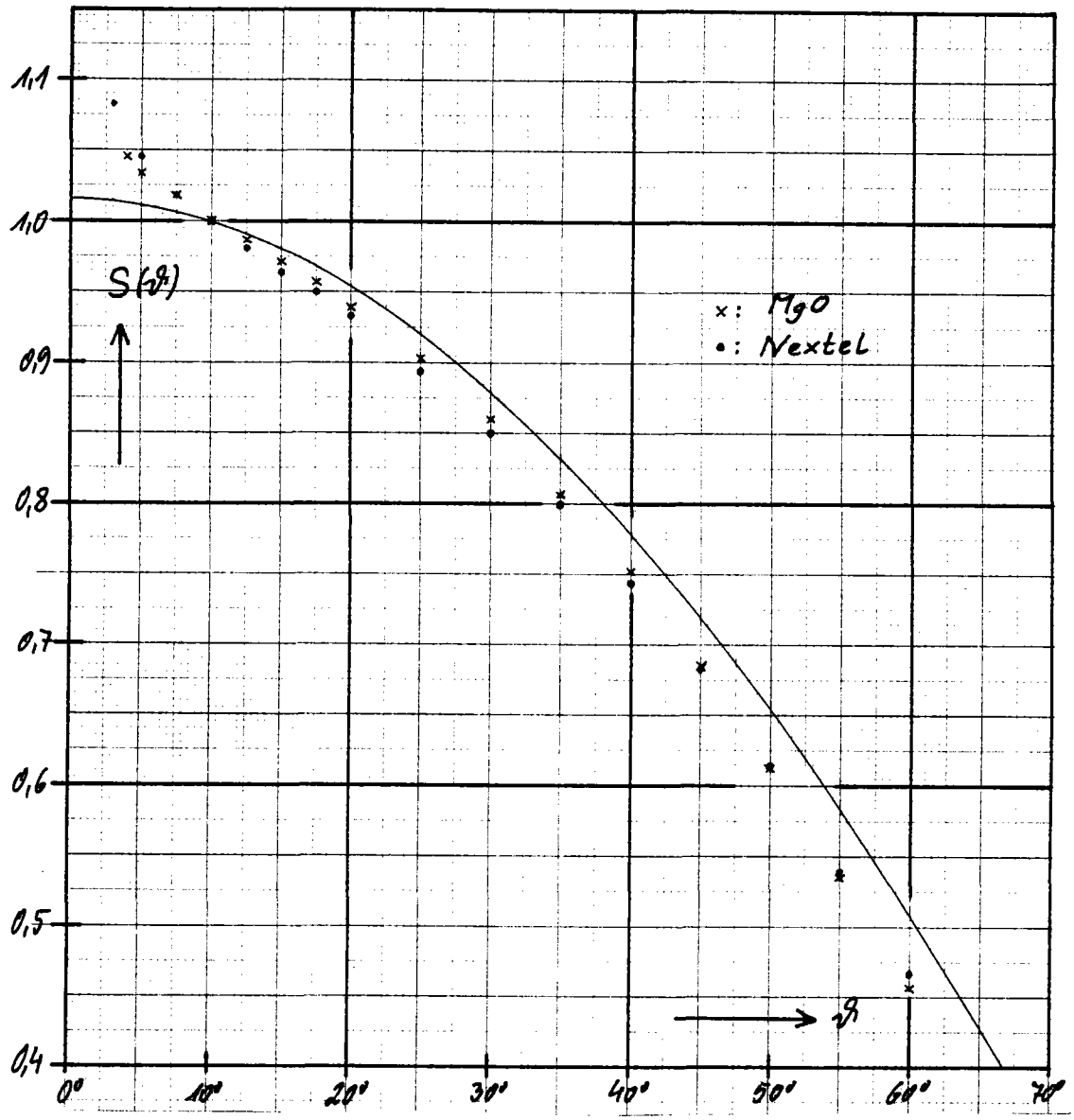

Fig. 1o Relative distribution of reflected radiation as function of the angle of observation for a white Nextel surface and for a magnesium oxid layer, compared with an ideal Lambertian distribution

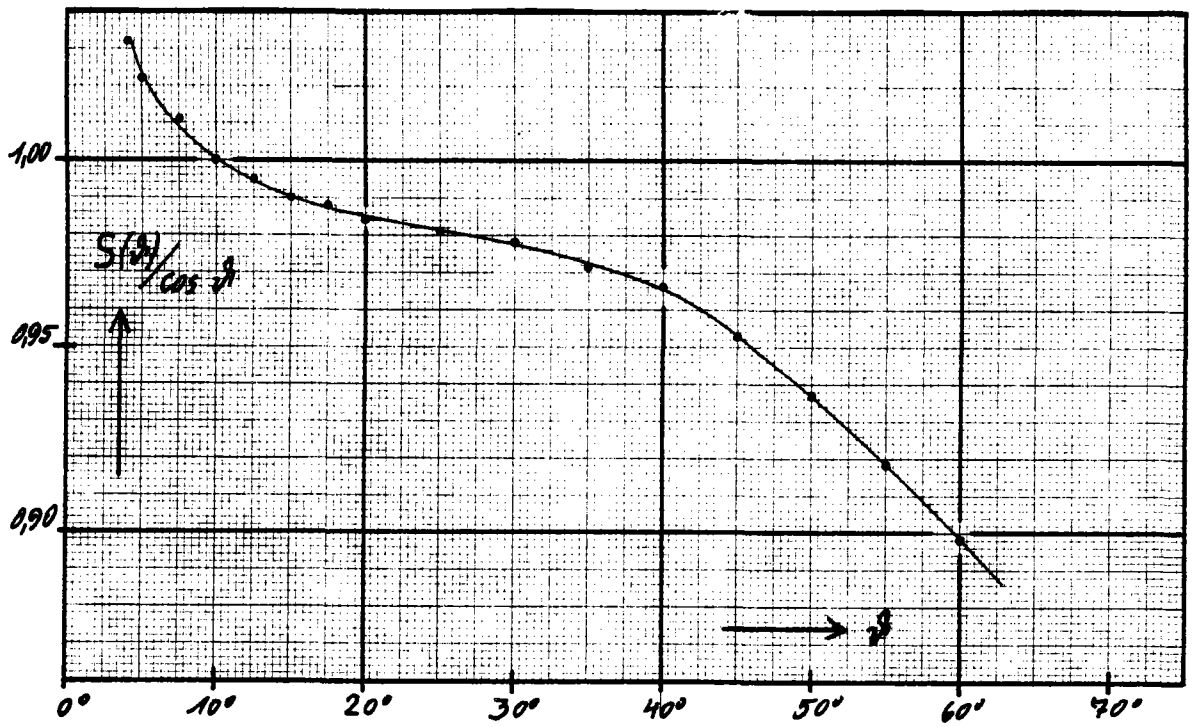

Fig. 11a Deviation from a cos-distribution for the radiation reflected on a magnesium oxid layer

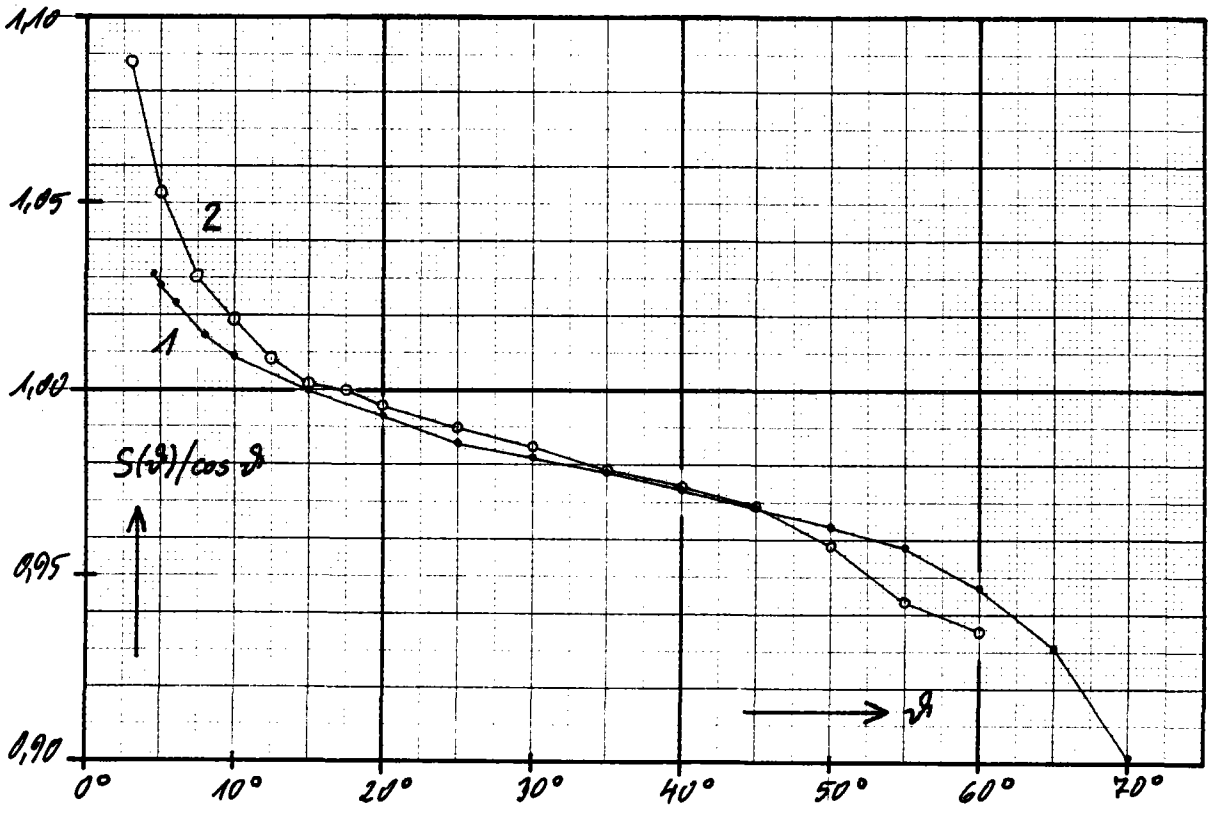

Fig. 11b Deviation from a cos-distribution for the radiation reflected on a Nextel layer; curve 1: direct signal of the previous measurement with reduced scale; curve 2: this measurement, referred to the cos of observation angle

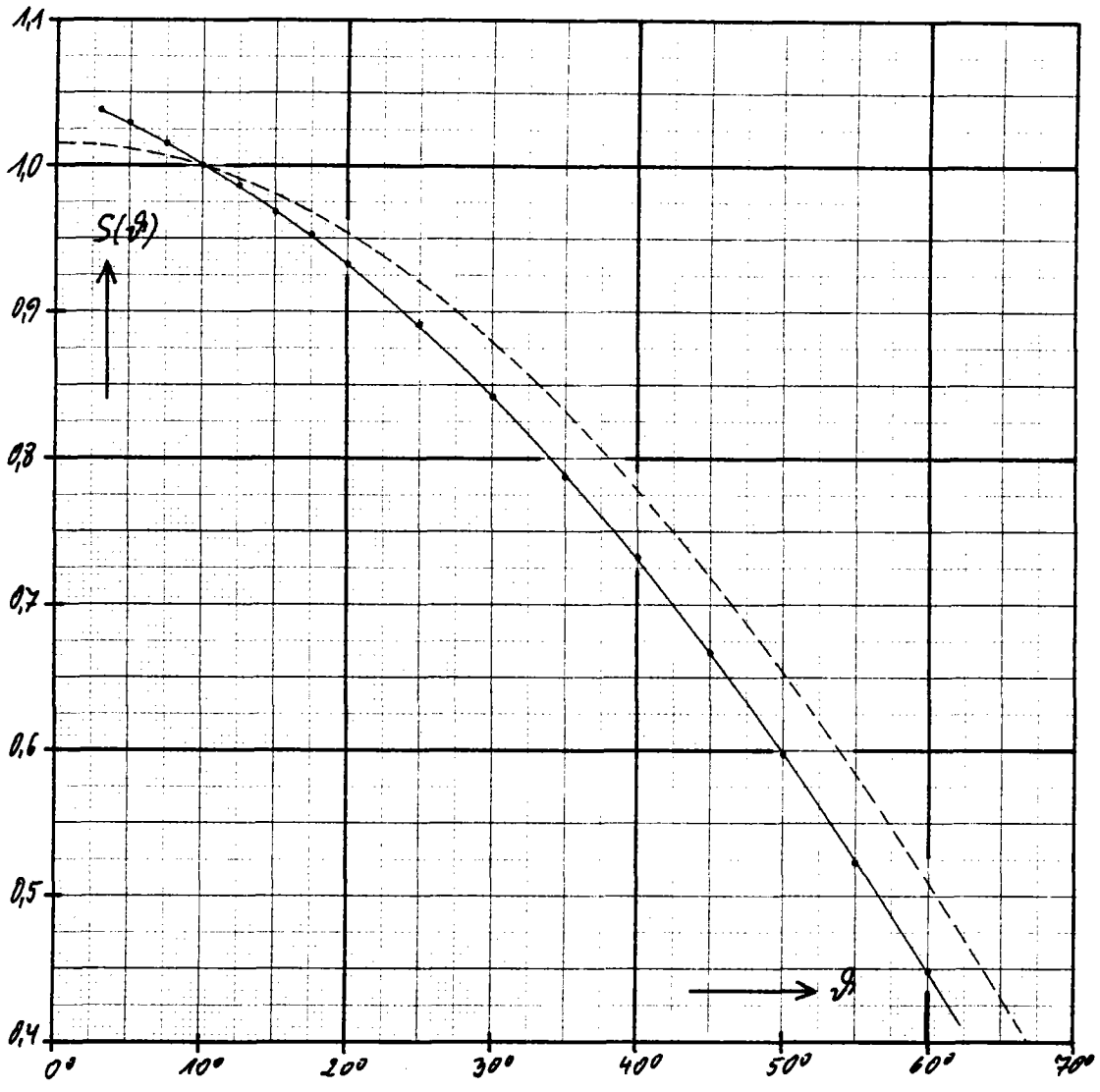

Fig. 12 Relative angular distribution of the radiation reflected on sample I, in comparison with the ideal Lambertian distribution

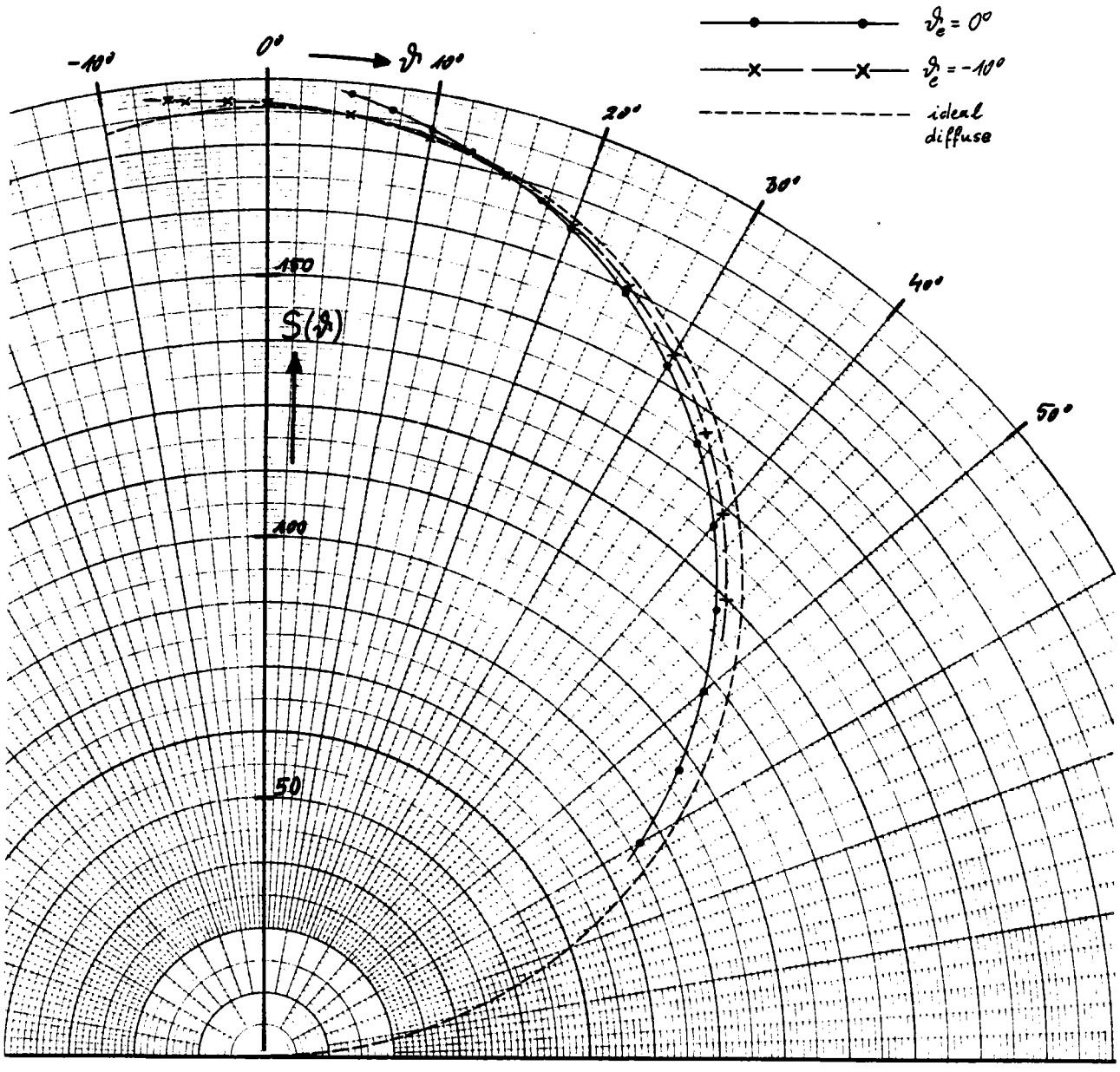

Fig. 13 Angular distribution of the reflectivity of sample I in polar diagram; angle of incidence: $\theta_e = 0^o$ and $\theta_e = -10^o$

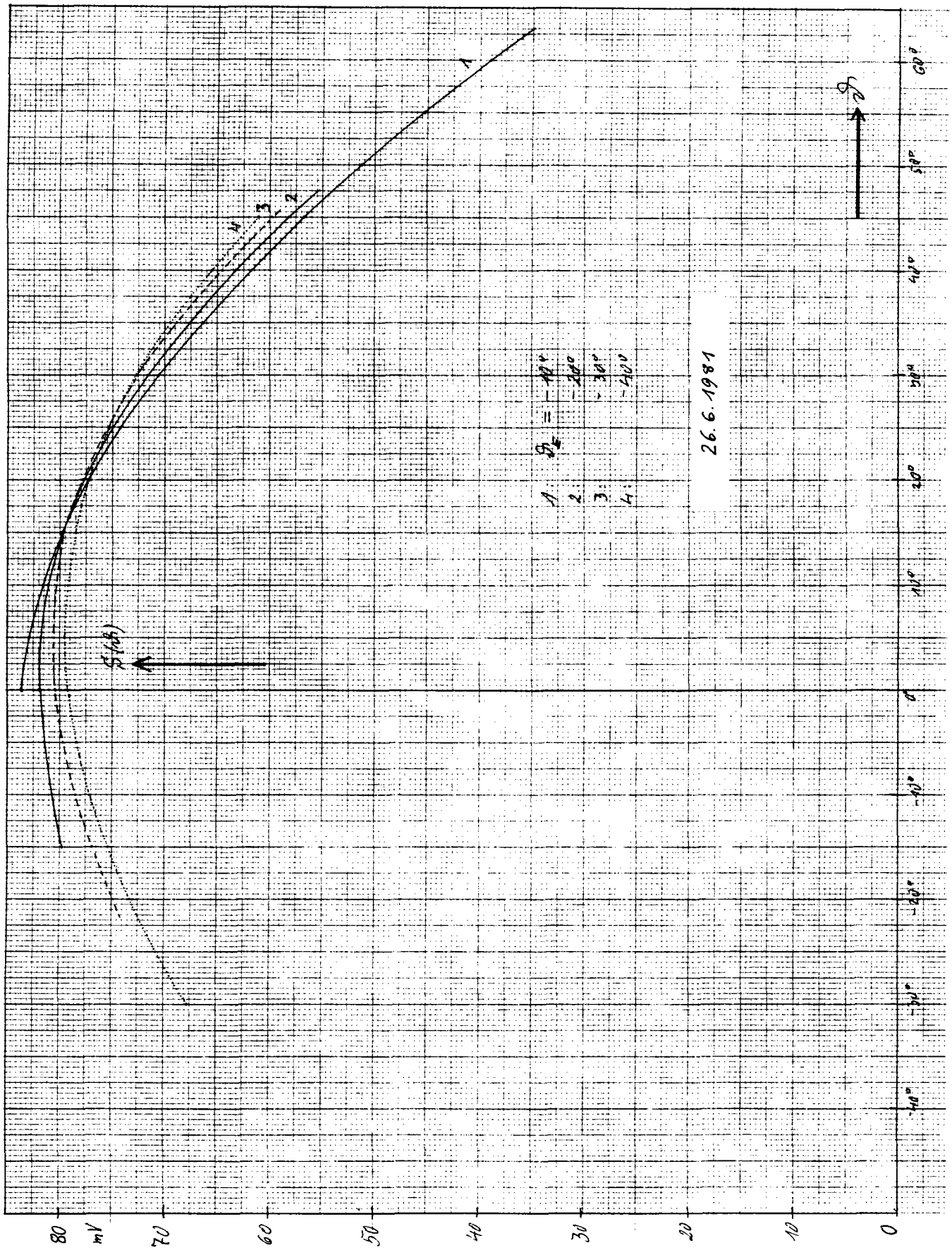

Fig. 14 Angular distribution of radiation reflected on sample I for different angles of incidence

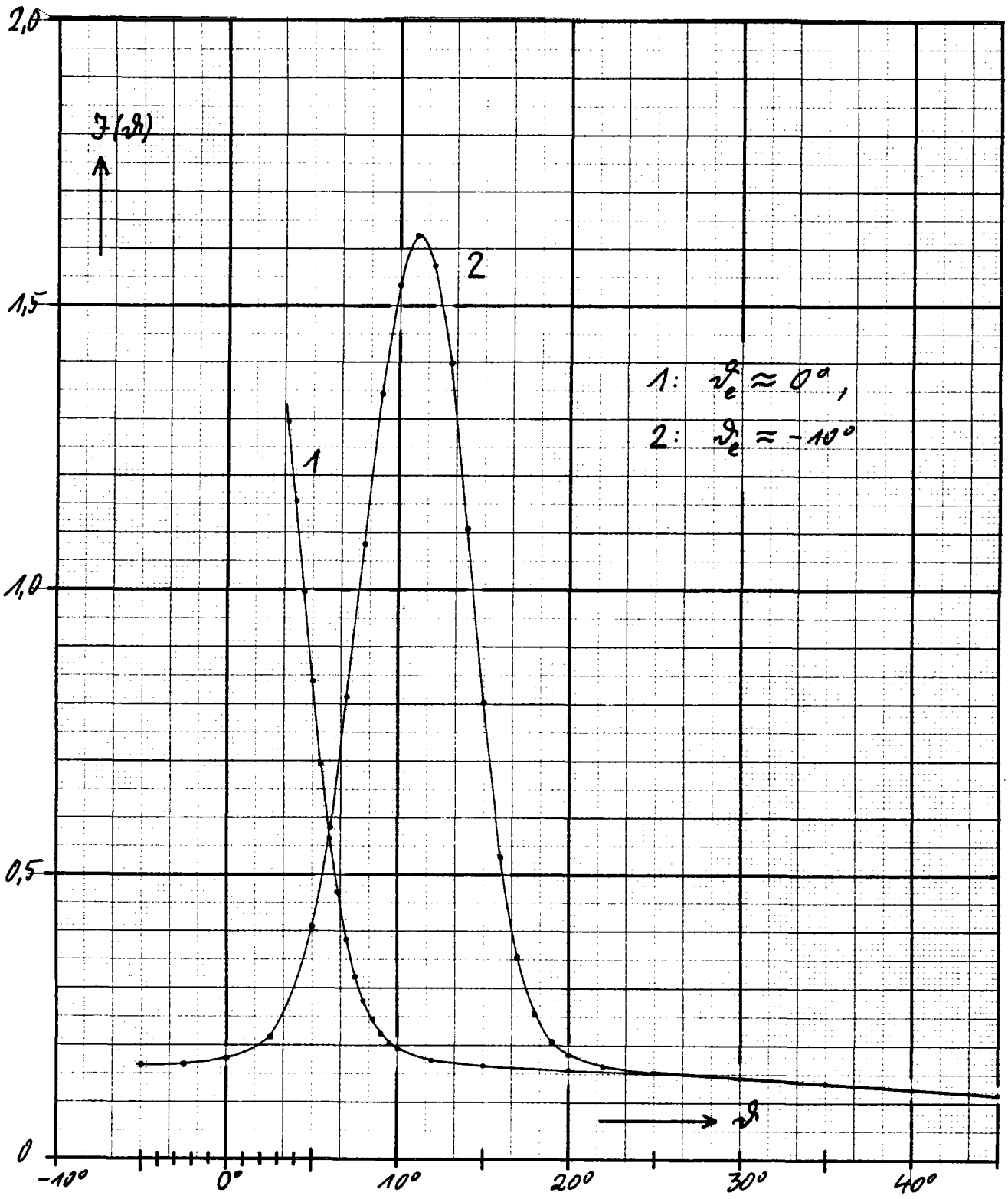

Fig. 15 Angular distribution of reflectivity, measured on sample II, for irradiation at $\theta_e = 0^o$ and $\theta_e = -10^o$

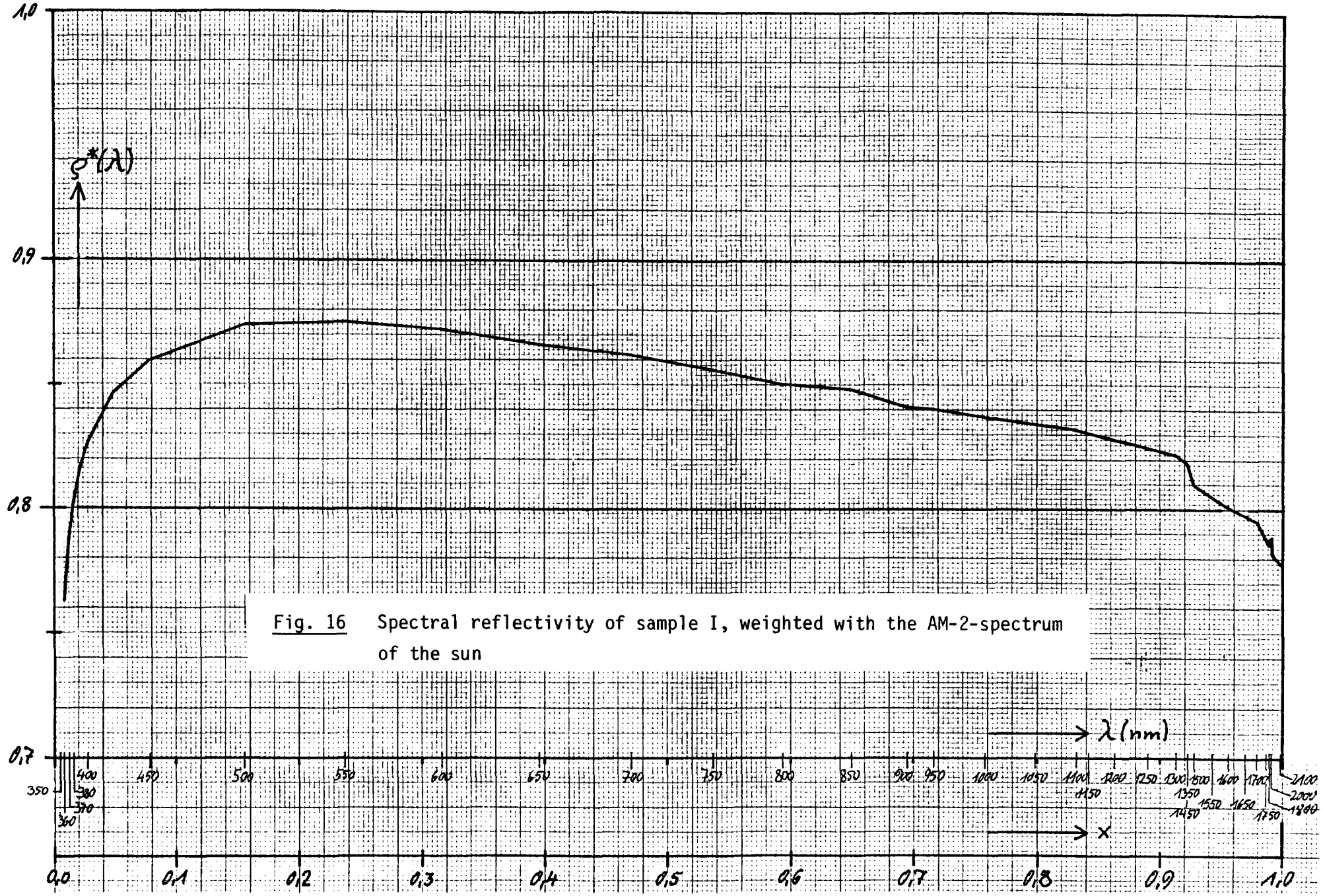

Fig. 16 Spectral reflectivity of sample I, weighted with the AM-2-spectrum of the sun

λ (nm):	I, 1a 26.3.81	I, 1b 14.4.81	II, 2a 17.3.81	II, 2b 15.4.81	III, 3a 17.3.81	III, 3b 14.4.81
360 nm	107,8%	104,4%	-	59,8%	-	71,5%
370	106,9	103,8	66,9%	66,9	78,9%	77,6
380	105,7	102,8	73,0	72,7	82,2	80,7
390	104,3	101,5	77,8	77,7	84,3	82,9
400	102,8	100,2	81,7	81,5	85,9	84,7
425	99,5	97,5	86,2	$85,9_5$	86,6	85,6
450	96,9	95,6	86,8	$86,5$	84,6	83,9
475	95,3	94,2	86,7	$86,5_5$	84,4	84,1
500	94,3	93,5	86,7	$86,6$	84,6	84,4
550	93,1	92,6	86,9	87,0	85,0	85,0
600	92,6	92,2	86,9	86,9	85,9	86,0
650	91,8	91,7	86,8	87,0	86,2	86,1
700	91,5	91,5	87,1	87,3	86,6	86,4
750	90,9	91,2	87,1	87,1	$86,6_5$	86,5
800	90,8	90,7	87,1	87,1	86,2	86,1
850	90,4	90,4	87,1	87,1	85,6	85,4
900	89,8	89,7	86,8	86,8	84,8	84,6
950	89,4	89,4	86,7	86,8	83,6	83,5
1000 nm	89,0	89,0	86,9	86,9	82,7	82,6
1100	88,5	88,5	86,9	86,9	81,9	81,9
1200	88,2	88,4	88,2	88,2	83,1	83,0
1300	88,0	88,0	88,3	88,2	83,4	83,3
1400	88,0	88,1	88,9	88,9	84,2	84,2
1500	88,0	88,0	88,5	88,5	84,4	84,2
1600	87,2	87,1	89,6	89,5	84,7	84,7
1700	86,7	86,8	89,8	90,0	85,0	84,9
1800	86,5	86,5	90,4	90,3	85,4	85,2
1900	88,0	88,3	92,1	92,3	87,3	87,2
2000	88,5	88,5	93,5	93,3	88,2	88,0
2100	88,7	88,7	93,7	93,7	88,3	88,1
2200	88,0	88,5	93,1	93,1	87,8	87,9
2300	89,6	89,6	94,9	95,0	89,8	89,6
2400	90,7	90,5	95,2	95,2	91,1	90,9
2500 nm	92,3%	92,1%	95,7%	95,8%	92,1%	92,0%

Table 1 Relative spectral reflectivity of sample I, II and III

λ (nm):	MgO ρ_{rel}	MgO ρ_{abs}	ρ_{abs} I, 1b'	ρ_{abs} II, 2b'	ρ_{abs} III, 3b'
36o nm	13o,o%	o,95o	o,763	o,437	o,523
37o	125,6	o,952	o,787	o,5o7	o,588
38o	122,1	o,953	o,8o2	o,567	o,63o
39o	118,8	o,955	o,816	o,625	o,666
4oo	115,9	o,957	o,827	o,673	o,699
425	11o,8	o,961	o,846	o,745	o,742
45o	1o7,4	o,966	o,86o	o,778	o,755
475	1o5,4	o,969	o,866	o,796	o,773
5oo	$1o3,9_5$	o,972	o,874	o,81o	o,789
55o	$1o3,o_5$	o,974	o,875	o,822	o,8o3
6oo	$1o2,8$	o,972	o,872	o,822	o,813
65o	$1o2,6_5$	o,969	o,866	o,821	o,813
7oo	$1o2,6_5$	o,967	o,862	o,822	o,814
75o	$1o2,8$	o,965	o,856	o,818	o,812
8oo	1o2,8	o,963	o,85o	o,816	o,8o7
85o	1o2,6	o,962	o,848	o,817	o,8o1
9oo	1o2,4	o,96o	o,841	o,814	o,793
95o	1o2,1	o,959	o,84o	o,815	o,784
1ooo nm	1o1,9	o,958	o,837	o,817	o,777
11oo	1o1,7	o,956	o,832	o,817	o,77o
12oo	1o1,8	o,954	o,828	o,827	o,778
13oo	1o1,9	o,952	o,822	o,824	o,778
14oo	$1o2,1_5$	o,95o	o,819	o,827	o,783
15oo	$1o3,o$	o,948	o,81o	o,815	o,775
16oo	1o3,o	o,947	o,8o1	o,823	o,779
17oo	1o3,2	o,945	o,795	o,824	o,777
18oo	$1o3,8_5$	o,944	o,786	o,821	o,774
19oo	1o5,6	o,942	o,788	o,823	o,778
2ooo	1o6,5	o,941	o,782	o,824	o,778
21oo	1o7,2	o,94o	o,778	o,822	o,773
22oo	1o6,9	o,939	o,777	o,818	o,772
23oo	1o7,7	o,937	o,78o	o,827	o,78o
24oo	1o8,6	o,936	o,78o	o,821	o,783
25oo nm	11o,8%	o,935	o,777	o,8o8	o,776

Table 2 Relative and absolute spectral reflectivity of magnesium oxide; absolute spectral reflectivity of sample I, II and III

ϑ (Grad):	$\vartheta_e = -1o^o$	$\vartheta_e = -2o^o$	$\vartheta_e = -3o^o$	$\vartheta_e = -4o^o$
- 4o				
- 35				
- 3o				67,8
- 25				7o,7
- 2o			74,9	73,3
- 15		79,8$_5$	76,9	75,4
- 1o		8o,7	78,5	77,1
- 5		81,5	79,7	78,4
o	83,6 mV	81,9 mV	8o,4 mV	79,2 mV
5	82,9	81,8	8o,6	79,5
1o	81,5$_5$	81,o$_5$	8o,3	79,2
15	79,8	79,7	79,7	78,5
2o	77,3	77,7	77,8	77,2
25	74,3	75,o	75,4	75,3
3o	7o,6	71,5$_5$	72,6	72,6
35	66,4	67,6	68,9	69,5
4o	61,8	63,2	64,5	65,5
45	56,8	58,2	59,8	61,1
5o	51,3			
55	45,3			
6o	39,o			
65	-			

Table 3 Bidirectional reflectance characteristics of sample I

ϑ (Grad):	1 N = 3 W	2 N = 5 W	3 (mit Filter)	1'	2'	3'
o	82,9 mV	18o,8 mV	7,6o mV	1,ooo	1,ooo	1,ooo
5	82,2	179,4	7,54	o,9916	o,9923	o,9921
1o	81,o	176,8	7,42	o,9777	o,9779	o,9763
15	79,2	172,8	7,26	o,9554	o,9558	o,9553
2o	76,9	167,5	7,o3	o,9276	o,9264	o,925o
25	73,9	16o,8	6,76	o,8914	o,8894	o,8895
3o	7o,2	152,9	6,42	o,8468	o,8457	o,8447
35	66,2	144,o	6,o6	o,7986	o,7965	o,7974
4o	61,7	133,8	5,62	o,7443	o,74oo	o,7395
45	56,5 mV	122,7 mV	5,16 mV	o,6815	o,6787	o,6789

Table 4 Angular distribution of radiation reflected on sample I (irradiation at $\vartheta_e = -10^o$) for the spectrum of a filament lamp at reduced power (column 1), at rated power (column 2), and with optical blue-green filter (column 3); columns 1', 2' and 3': distribution normalized on $S(\vartheta = 0^o)$.

λ (nm):	1 26.3.81	2 14.4.81	3a T = 3o °C 7.7.81	3b T = 1oo °C 7.7.81	3c T = 13o °C 7.7.81	3d T = 3o °C 7.7.81	4 T = 3o °C 29.7.81
36o nm	1o7,8%	1o4,4%	-	-	-	-	1o5,o%
37o	1o6,9	1o3,8	1o5,9%	1o4,5	1o3,9%	1o4,6%	1o4,6
38o	1o5,7	1o2,8	1o4,8	1o3,6	1o2,9	1o3,6	1o3,6
39o	1o4,3	1o1,5	1o3,5	1o2,4	1o1,8	1o2,2	1o2,5
4oo	1o2,8	1oo,2	1o1,9	1o1,o	1oo,5	1o1,o	1o1,1
425	99,5	97,5	99,1	98,2	97,9	97,9	$98,4_5$
45o	96,9	95,6	96,5	96,o	95,7	95,7	$96,2_5$
475	95,3	94,2	94,5	94,4	94,2	94,1	$94,7_5$
5oo	94,3	93,5	93,4	93,3	93,1	93,2	93,8
55o	93,1	92,6	92,2	92,3	92,2	92,2	92,8
6oo	92,6	92,2	91,5	91,6	91,7	91,6	$92,1_5$
65o	91,8	91,7	91,o	91,1	91,2	91,o	91,5
7oo	91,5	91,5	9o,9	91,o	91,o	9o,9	91,3
75o	9o,9	91,2	9o,5	9o,6	9o,7	9o,6	91,o
8oo	9o,8	9o,7	9o,2	9o,4	9o,4	9o,1	9o,6
85o	9o,4	9o,4	89,8	89,9	9o,o	89,8	9o,3
9oo	89,8	89,7	89,1	89,4	89,5	89,2	89,6
95o	89,4	89,4	88,6	88,9	88,9	88,7	89,2
1ooo nm	89,o%	89,o%	88,4%	88,6%	88,5%	88,4%	88,9%
11oo	88,5	88,5	87,9	88,1	88,o	88,o	88,4
12oo	88,2	88,4	87,7	87,9	87,7	87,7	88,2
13oo	88,o	88,o	87,4	87,5	87,4	87,4	87,9
14oo	88,o	88,1	87,5	87,7	87,6	87,6	87,9
15oo	88,o	88,o	87,5	87,7	87,7	87,5	87,9
16oo	87,2	87,1	86,7	86,7	86,7	86,8	87,1
17oo	86,7	86,8	86,1	86,4	86,3	86,2	86,5
18oo	86,5	86,5	85,9	86,o	86,1	85,9	86,4
19oo	88,o	88,3	87,7	88,o	88,o	87,7	87,4
2ooo	88,5	88,5	88,o	88,5	88,4	88,1	87,7
21oo	88,7	88,7	88,1	88,5	88,4	88,1	88,3
22oo	88,o	88,5	87,7	87,9	88,o	87,5	87,8
23oo	89,6	89,6	89,1	89,3	89,3	89,o	89,2
24oo	9o,7	9o,5	89,8	9o,2	9o,4	9o,o	89,7
25oo nm	92,3%	92,1%	91,4%	92,1%	92,3%	91,7%	91,o%

Table 5 Relative spectral reflectivity of sample I at room temperature (columns 1,2, 3a, 3d and 4) and at elevated temperatures (columns 3b and 3c)

ϑ (Grad):		1 13.4.81	2 24.6.81	3a T = 25 °C 1o.7.81	3b T = 1oo °C	3c T = 15o °C
o		182,8 mV	82,9 mV	85,2 mV	85,5 mV	86,2 mV
5		$181,4_5$	82,2	84,5	84,7	85,4
1o		$178,8_5$	81,o	83,3	83,4	84,1
15		175,2	79,2	81,6	81,5	82,4
2o		169,8	76,9	79,o	79,1	79,9
25		$163,1_5$	73,9	76,o	76,o	76,7
3o		155,4	7o,2	72,3	72,3	73,o
35		146,3	66,2	68,o	68,o	68,7
4o		136,3	61,7	63,3	63,4	64,o
45		124,7 mV	56,5 mV	58,o	58,1	58,7
5o				52,5	52,6	53,2
55				46,3	46,4	47,o
6o				39,8	39,9	4o,4
65				33,4 mV	33,4 mV	33,7 mV
	cos ϑ	1'	2'	3a'	3b'	3c'
o	1,ooo	1,ooo	1,ooo	1,ooo	1,ooo	1,ooo
5	o,9962	o,9923	o,992	o,992	o,991	o,991
1o	o,9848	o,9784	o,978	o,978	o,975	o,976
15	o,9659	o,9584	o,955	o,958	o,953	o,956
2o	o,9397	o,9289	o,928	o,927	o,925	o,927
25	o,9o63	o,8925	o,891	o,892	o,889	o,89o
3o	o,866o	o,85o1	o,847	o,849	o,846	o,847
35	o,8192	o,8oo3	o,799	o,798	o,795	o,797
4o	o,766o	o,7456	o,744	o,743	o,742	o,742
45	o,7o71	o,6822	o,682	o,681	o,68o	o,681
5o	o,6428			o,616	o,615	o,617
55	o,5736			o,543	o,543	o,545
6o	o,5ooo			o,467	o,467	o,469
65	o,4226			o,392	o,391	o,391

Table 6 Angular reflectance characteristics of sample I (irradiation at $\vartheta_e = -\ 1o^o$) at room temperature and at elevated temperature

DISTRIBUTION LIST

1)	SSPS-MEMBER COUNTRY REPRESENTATIVES (EXECUTIVE COMMITTEE AND T+O ADVISORY BOARD)	L. REY (EC CHAIRMAN)	
		G. FANINGER	(A)
		H. KLEINRATH	(A)
		J. DELCROIX	(B)
		A. MICHEL	(B)
		P. KESSELRING	(CH)
		C.J. WINTER	(D)
		M. FISCHER	(D)
		W. HOFMANN	(D)
		A. MUNOZ TORRALBO	(E)
		C. ORTIZ	(E)
		E. CARABATEAS	(GR)
		F. REALE	(I)
		G. BEER	(I)
		L. BRANDELS	(S)
		J. HOLMBERG	(S)
		G. BRAUN	(USA)
2)	IEA - SECRETARIAT	L. BOXER	
3)	R M F T	H. KLEIN H. HEINZELMANN	
4)	C E E	I. MARTIN	
5)	SANDIA LABORATORIES	A. BAKER	
6)	D F V L R	R. KÖHNE	
7)	OPERATING AGENT	M. BECKER F. DIESSNER H. ELLGERING W. GRASSE P. HEINTZELMANN A. KALT W. VON KRIES	
8)	INTERNATIONAL TEST & EVALUATION TEAM	C. SELVAGE	(10 x)
9)	SEVILLANA	F. RUIZ	(3 x)
10)	ACUREX CORP.	A.F. SCHRAUB	
11)	ANSALDO	G. TOMEI	
12)	BELGONUCLEAIRE	G. DEBIER	
13)	INTERATOM	B. FLOSS	
14)	MAN - NEUE TECHNOLOGIE	J. FEUSTEL J.P. KEMPER	
15)	MARTIN MARIETTA CORP.	P. BROWN	
16)	SAIT	S. MUSCH	
17)	SNAMPROGETTI	C. MICHELI	
18)	TECNICAS REUNIDAS	M. LOPEZ	